Improving molecular orientation by optimizing relative delay and intensities of two-color laser pulses

Je Hoi Mun[1,*] and Hirofumi Sakai[2,3,†]

[1]*Center for Relativistic Laser Science, Institute for Basic Science (IBS), Gwangju 61005, Republic of Korea*
[2]*Department of Physics, Graduate School of Science, The University of Tokyo, 7-3-1 Hongo, Bunkyo-ku, Tokyo 113-0033, Japan*
[3]*Institute for Photon Science and Technology, Graduate School of Science, The University of Tokyo,
7-3-1 Hongo, Bunkyo-ku, Tokyo 113-0033, Japan*

We numerically explore molecular orientation dynamics with moderately intense nanosecond two-color laser pulses. It is believed that the nanosecond two-color pulse can adiabatically control the molecular orientation. However, in our simulation based on the time-dependent Schrödinger equation, which naturally includes nonadiabatic effects, the orientation dynamics shows clear deviations from the adiabatic approximation (AA) results, while the molecular alignment dynamics is in good agreement with the AA results. The nonadiabaticity is significantly influenced by three parameters, the intensities, and the relative delay of the two wavelengths. In this work, we clarify the reason behind the nonadiabaticity and provide the solutions for achieving higher degrees of orientation.

I. INTRODUCTION

Techniques for controlling the rotation of molecules provided opportunities to observe various phenomena related to anisotropic structures of molecules. The controlling techniques have been applied for experiments such as optimal control of multiphoton ionization [1] and molecular imaging based on high-order harmonic generation [2–5]. Controlling the rotational motion of the molecule is referred to as "alignment" or "orientation." The molecules are considered to be "aligned" when the molecular fixed axis is synchronized with respect to a laboratory fixed axis with the directional plus-minus inversion symmetry. If the aligned molecules are under the additional head-versus-tail order confinement, it is considered to be "oriented" (see Fig. 1).

There were theoretical [6–8] and experimental [9,10] demonstrations of the alignment, where an intense nonresonant laser field was applied. The laser field with the moderately strong intensity (10^{11}–10^{13} W/cm^2) generates an induced dipole in the molecule. The induced dipole is generally anisotropic. As a result, if a vector component of the induced dipole along a molecular axis is larger than the other components, the molecular axis is synchronized with respect to the polarization of the laser field. In the adiabatic regime [6,7], where the pulse width of the laser is much longer than the molecular rotational period, the molecules are aligned during the presence of the laser field, and they return to their initial free-rotor states after the laser field is turned off. In contrast, in the impulsive (nonadiabatic) regime [11–16], an ultrashort laser pulse excites an initial rotational quantum state into a broadly excited rotational superposition via Raman

mechanism. After the laser pulse has passed, the excited rotational superposition exhibits periodic "revival" features of the molecular alignment.

The laser-based alignment has been well studied both theoretically and experimentally. However, techniques for the orientation still are developing with remaining challenges. Traditional methods for the orientation were the brute-force orientation [17,18] and the hexapole focusing [19], which were based on the interactions between a strong electrostatic field and the intrinsic permanent dipole moment of the molecule. For laser-field-based techniques, supported by theoretical studies [20,21], a method using "a combination of electrostatic and linearly polarized nonresonant laser fields" (combined field) was demonstrated in the adiabatic regime [22,23]. The combined-field technique was employed also for the three-dimensional orientation of asymmetric top molecules by using the elliptically polarized laser field [24]. As an all-optical molecular orientation method, a nonresonant phase-locked two-color laser field was proposed in [25] and demonstrated experimentally in [26]. Moreover, owing to the advance of THz laser pulse techniques, orientation methods using the THz pulses were also reported [27–29].

In spite of the above achievements, there are still two critical difficulties in improving the degrees of molecular orientation. One of these difficulties is related to the initial rotational states of the molecule. In earlier experiments, the degrees of orientation were observed from molecules in thermal ensembles. The reported degrees of orientation, which are defined as the averages over various initial rotational quantum states, were modest due to the following reason: depending on the initial rotational state, there are two possible orientations, either to one direction of the field polarization or to its opposite, which leads to the significantly reduced net degree of orientation. To overcome this problem, the initial rotational states of molecules were selected before they were used as a molecular sample.

---

*mun1219@ibs.re.kr
†hsakai@phys.s.u-tokyo.ac.jp

013404-1
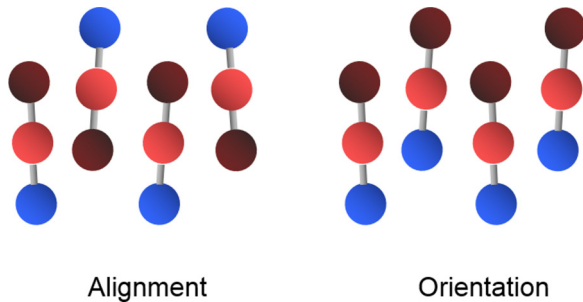
FIG. 1. Molecular alignment and orientation.

FIG. 2. Temporal profiles of two-color laser pulses. Right and left panels illustrate the two-color laser pulses with and without a delay between the two wavelengths. The two-color laser pulses with the optimal delay can give rise to higher degrees of orientation than those with the zero delay.

State-selected NO molecules by a hexapole focuser were oriented with a combination of electrostatic and femtosecond laser fields [30]. Additionally, for selecting rotational states of asymmetric top molecules, which are the most general type of molecules from the geometrical classification, a molecular deflector generating "a two-wire field" was used [31–34]. Usages of the state-selected molecules in the experiments improved the degrees of orientation (see [30–34]).

Another crucial issue on the molecular orientation is related to the adiabaticity in the orientation dynamics. The importance of the adiabatic orientation in the two-color laser pulse technique [35] and the combined-field technique [36] was demonstrated by numerical simulations. It was shown that the adiabatic process makes it more advantageous to achieve much higher degrees of molecular orientation. However, a drawback of the adiabatic process is that the orientation is attainable only in the presence of the applied laser field. For exploiting the advantage of the adiabatic orientation even in the laser-field-free condition, a laser pulse with a slow turn on and a rapid turn off has been applied in the presence of a weak electrostatic field [33,34,37].

In recent studies, the analyses for clarifying the importance of the adiabaticity in the orientation dynamics have been revisited from the perspective of "pendular states" based on the time-dependent Schrödinger equation (TDSE) [38–42]. For the asymmetric top molecules, nonadiabatic transitions between the pendular states in the combined-field technique have been investigated [38–40]. For the ground-state OCS molecules, nonadiabatic transitions between the "pendular doublet," which is a pair of quantum states oriented oppositely, has been investigated in the combined-field technique [41,42]. These studies also pointed out that the crossed angle between the polarization directions of the electrostatic and the laser fields is an important parameter. The parallel-polarized field condition provides the best adiabaticity in the molecular orientation, while near 90-degree crossed polarizations result in dominant nonadiabatic dynamics.

In the two-color laser field technique, the crossed angle between the two polarizations plays the same role as in the combined-field technique. The adiabaticity in the molecular orientation dynamics is expected to be maximized with the parallel-polarized two-color laser fields. In addition to this, for further enhancement of the adiabaticity, it is necessary to optimize other optical conditions, the intensities and the relative delay of the two wavelengths. Figure 2 schematically illustrates nanosecond two-color laser pulses with the pulse widths of about 10 ns. Let us assume that we observe the degrees of alignment and orientation at the peak of the 2ω pulse. As shown in the present study, the degree of molecular alignment increases with the total intensity of the two-color laser field. Thus the strongest molecular alignment is achieved if the peaks of the two laser pulses coincide temporally, as shown in Fig. 2(left). However, the optimal condition for the orientation is not the same as that for the alignment. A two-color pulse with a proper delay between the two wavelengths [Fig. 2(right)] can give rise to much higher degrees of molecular orientation. Such an orientation dynamics is never explainable with the adiabatic approximation (AA).
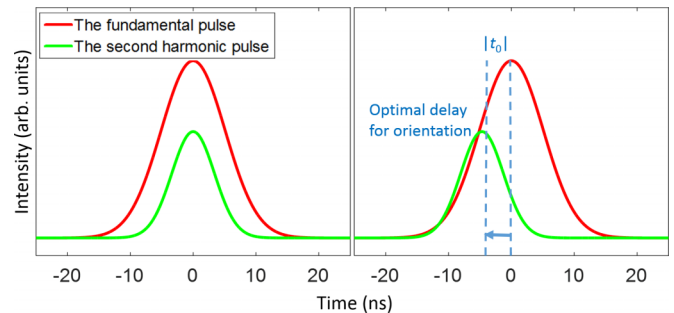
In this work, we explore the nonadiabatic effects taking place in the rotational ground state of the OCS molecule, which is irradiated with a two-color nonresonant laser field. We take into account a practical experimental condition where the second harmonic pulse has a shorter pulse width than the fundamental pulse due to the nonlinear generation process of the second harmonic. We explore how the orientation dynamics is influenced by the intensities and the delay of the two wavelengths, when the pulse widths are fixed as constants. From those parameter dependences, we provide recipes for the best molecular orientation in the two-color laser field technique.

This paper is organized as follows. In Sec. II, we review the numerical model for describing the molecular orientation by the two-color laser field. The modeled TDSE is solved by time-dependent unitary transformation method for rapid numerical calculations. Details of the method are given in the Appendix. In Sec. III, we discuss the orientation dynamics of the OCS molecule from the TDSE and the AA. With the fixed pulse widths, the intensities and the relative delay of the two wavelengths are varied. The nonadiabatic behaviors of the rotational wave packets are investigated. We analyze the origin of the nonadiabaticity and provide recipes for achieving higher degrees of orientation from theoretical and practical aspects. In Sec. IV, we present a summary of the paper and an outlook.

II. NUMERICAL METHOD

In this section, we describe the theoretical background of the rigid-rotor model dealing with the rotational dynamics of molecules. In the regime of laser intensities 10^{10}–10^{12} W/cm^2, the electronic and vibrational structures can be described by

low-order perturbation theory. By assuming the molecule as a rigid rotor, the molecular system has only rotational degrees of freedom. The rigid-rotor Hamiltonian of a linear polar molecule is given by

$$H_{\text{rot}} = B\vec{J}^2, \qquad (1)$$

where B is the rotational constant of the molecule, $\vec{J}^2$ the squared angular momentum operator. The interaction between the electric fields and the rigid rotor is given by

$$H_{\text{int}} = -\sum_i \mu_i E^i - \frac{1}{2!}\sum_{ij} \alpha_{ij} E^i E^j$$
$$- \frac{1}{3!}\sum_{ijk} \beta_{ijk} E^i E^j E^k - \dots, \qquad (2)$$

where μ is a permanent dipole moment vector, α a polarizability tensor, and β a hyperpolarizability tensor.

We consider a linearly polarized and phase-locked nonresonant two-color laser field. The laser field is given by

$$E(t) = E_\omega(t)\cos(\omega t) + E_{2\omega}(t - t_0)\cos(2\omega t + \phi), \qquad (3)$$

where $E_\omega(t) \equiv E_{\omega,0}\exp(-t^2/2\tau_\omega^2)$ and $E_{2\omega}(t) \equiv E_{2\omega,0}\exp(-t^2/2\tau_{2\omega}^2)$ are the envelopes of the ω and 2ω fields with $E_{\omega(2\omega),0}$ being the peak strength of the field, and $\tau_{\omega(2\omega)}$ is related to the $\text{FWHM} = 2\tau_{\omega(2\omega)}\sqrt{2\ln 2}$. ϕ is the phase difference between the two wavelengths. t_0 is the temporal delay of the two envelopes (see the right panel of Fig. 2).

Assuming that the oscillation frequencies of the laser fields ω and 2ω are far from any molecular resonance and much higher than the rotational frequency of the molecule, we average over the rapid oscillations of the nonresonant laser field. Then the permanent dipole interaction vanishes. On the other hand, the second and the third interaction terms in Eq. (2) are written as

$$H_{\text{int}}(t) = -\frac{1}{4}[E_\omega(t)^2 + E_{2\omega}(t - t_0)^2](\alpha_{zz} - \alpha_{xx})\cos^2\theta$$
$$- \frac{1}{8}[\cos\phi E_\omega(t)^2 E_{2\omega}(t - t_0)]$$
$$\times [(\beta_{zzz} - 3\beta_{zxx})\cos^3\theta + 3\beta_{zxx}\cos\theta], \qquad (4)$$

where θ is the polar angle between the molecular axis and the laser polarization. In Eq. (4) we omitted the terms independent of θ, which represent only the energy shifts. α_{zz} and α_{xx} are the polarizability components parallel and perpendicular to the molecular axis, while β_{zzz} and β_{zxx} are hyperpolarizability components parallel and perpendicular to the molecular axis. These constants for the OCS molecule are taken from [43].

The molecular alignment is brought by the first term in Eq. (4). In the θ space, this interaction makes a binding potential with two identical valleys localized at $\theta = 0$ and $\theta = \pi$. The depth of the valleys is determined by the total intensity of the irradiated laser fields. The second term in Eq. (4) has an asymmetry in the θ space so that the valley at $\theta = 0$ becomes deeper than the other one at $\theta = \pi$. This asymmetric term is smaller than the alignment term typically by two orders of magnitude. We fix $\phi = 0$ for the rest of the paper. Using the time-dependent Hamiltonian given by Eqs. (1) and (4), we solved the time-dependent Schrödinger equation. The numerical method is given in the Appendix.

III. NUMERICAL RESULTS

A. Nonadiabaticity in the molecular orientation by two-color laser fields

In this work, we calculate the time evolution of the ground-state OCS molecules, which are irradiated with the fundamental (ω) and its second harmonic (2ω) laser pulses whose pulse widths are 12 and 8 ns, respectively, by FWHM. The peak intensities and the delay of the two wavelengths are varied. For the various conditions, the degrees of alignment $\langle\cos^2\theta\rangle$ and orientation $\langle\cos\theta\rangle$ are evaluated at the peak of the 2ω laser pulse. Figure 3 shows the degrees of alignment and orientation, which are plotted by contour images as a function of the delay and the peak intensity of the ω pulse. The peak intensities of the 2ω pulse are fixed as 8.0×10^{10} and 6.0×10^{11} W/cm^2 for Figs. 3(1) and 3(2), respectively. The negative delay means the ω is delayed from the 2ω.

In the contour images for the alignment shown in the right panels of Fig. 3, all results exhibit semielliptical structures, which indicate that the molecules are better aligned with the higher total intensity of the two laser pulses. For the alignment, the TDSE results are in good agreement with those from the AA. For the orientation from the AA, the images show the similar semielliptical structures. In sharp contrast to the results for the alignment, the images from the TDSE calculations exhibit "banana-shaped" structures, which are not in agreement with the AA results. The nonadiabaticity in the orientation dynamics is influenced by the intensities and the delay of the two pulses.

In Fig. 4, for observing the detailed rotational dynamics, we plot the degrees of alignment and orientation (left) and populations of two pendular states (right) as a function of time. The two pendular states are the two lowest-lying eigenstates of the field-dressed Hamiltonian. The dynamics is investigated for four characteristic conditions labeled by (a)–(d) in Fig. 3(1). In the case of (a), where the delay is zero and the peak intensity of the ω is the highest at 10×10^{11} W/cm^2, while the peak intensity of 2ω is considerably low at 8.0×10^{10} W/cm^2, the achieved degree of orientation $\langle\cos\theta\rangle$ at the peak of the 2ω pulse is ~ 0.7. This value is far below the degree obtained from the AA, i.e., $\langle\cos\theta\rangle \sim 0.9$. We analyze the nonadiabaticity by projecting the time-dependent rotational wave packet into the two pendular states at each time step. The projected pendular populations must be conserved if the interaction process is purely adiabatic. In the numerical result shown in the right panel of Fig. 4(a), from $t = -9$ ns to $t = -6$ ns, 11% of the pendular ground state $|0,0\rangle_p$ has transferred into the oppositely oriented, the first excited pendular state $|1,0\rangle_p$.

The nonadiabatic dynamics is caused by a delayed creation of the orientation potential with respect to the alignment potential. The delay is a result of the temporal mismatch of the rising parts of the two laser pulses. As it is illustrated in Fig. 5, before the 2ω pulse interacts with the molecules, not the orientation but only the adiabatic alignment with the degree $\langle\cos^2\theta\rangle \sim 0.7$ is achieved by the ω field already at $t = -10$ ns. At this moment, the same amounts of rotational wave packets are bound to the two valleys located in $\theta = 0$ and $\theta = \pi$. During the alignment, the pendular ground and the excited states are degenerate. When the 2ω field starts to increase from $t \sim -10$ ns, the asymmetry between the two valleys is
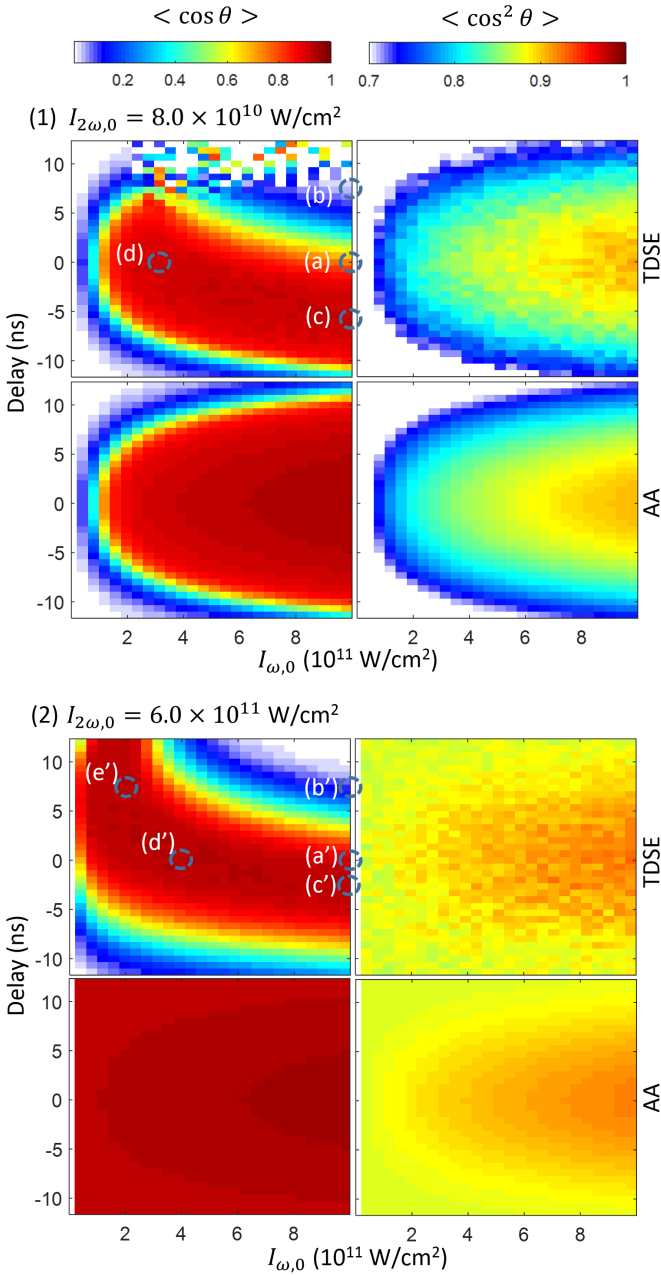
FIG. 3. The degrees of orientation (left) and alignment (right) observed at the peak of the 2ω pulse. The horizontal axis is the peak intensity of the ω pulse, while the vertical axis is the delay between the ω and 2ω pulses. The peak intensity of the 2ω pulse is fixed at either 8.0×10^{10} W/cm² (1) or 6.0×10^{11} W/cm² (2). The TDSE and AA results are shown.

FIG. 4. Temporal evolutions of the degrees of orientation and alignment (left) and the populations of the two lowest-lying pendular states (right). In the left panels, the left vertical axis of each panel represents $\langle \cos\theta \rangle$ or $\langle \cos^2\theta \rangle$, while the right vertical axis of each panel represents the intensities of the ω and the 2ω pulses in units of 10^{11} W/cm². In the right panels, the left vertical axis represents the populations of the two lowest-lying pendular states, while the right vertical axis of each panel represents the intensities of the ω and the 2ω pulses in units of 10^{11} W/cm². The four different conditions labeled by (a), (b), (c), and (d) in Fig. 3(1) are employed.

created. In the asymmetric potential, the ground pendular state $|0,0\rangle_p$ is no more degenerate with the first excited pendular state $|1,0\rangle_p$. The wave packet of the pendular ground state is located in the deeper potential valley. Meanwhile, the first excited pendular state $|1,0\rangle_p$ corresponds to the wave packet bound to the shallower valley. If the time evolution of the wave packet is adiabatic, the wave packet must be located in the deeper valley in the presence of the two-color laser field. However, the wave packet confined to the shallower potential before $t \sim -10$ ns imperfectly tunnels through the wall between the two valleys.

This difficulty in the tunneling between the valleys results in the nonadiabatic transition between the two pendular states.

The nonadiabatic transition becomes even more serious when the 2ω pulse is delayed from the ω pulse by 6.6 ns as it is shown in Fig. 4(b). Because of the delay, long before the 2ω pulse arrives, the relatively higher degree of alignment with $\langle \cos^2\theta \rangle \sim 0.8$ is achieved at $t = -8$ ns. With the subsequently increasing 2ω field, the molecules start to be oriented from $t = -8$ ns to $t = -6$ ns. However, the rotational wave packets bound to the shallower valley at $t = -8$ ns hardly move toward the deeper valley. From the perspective of the nonadiabatic transition, 47% of the pendular ground state $|0,0\rangle_p$ is transferred into the state $|1,0\rangle_p$.

To prevent the nonadiabatic transitions, conceivable two measures are as follows. (i) Synchronize the rising parts of
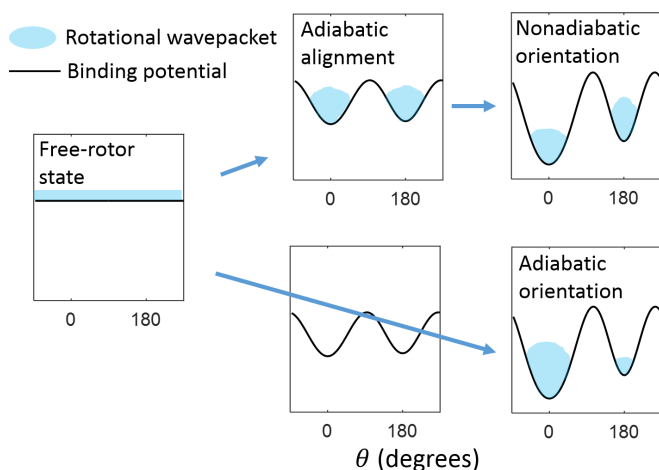
FIG. 5. Schematic illustrations of the orientation processes. The upper path shows a nonadiabatic orientation process, for which the orientation is preceded by the strong adiabatic alignment. The lower path shows an adiabatic orientation process, which could be achieved by forming the alignment and orientation potentials in harmony with each other.

the two pulses by introducing an appropriate delay. (ii) Avoid too strong alignment before the orientation by reducing the intensity of the ω pulse. The two measures (i) and (ii) are achieved in the conditions (c) and (d). In Figs. 4(c) and 4(d), improvements of the adiabaticity are observed and higher degrees of orientation with $\langle \cos \theta \rangle > 0.9$ are achieved. For the case of Fig. 4(c), where the ω pulse is delayed by 6.0 ns from the 2ω pulse, the two pulses are well synchronized in their rising parts. The alignment and orientation start to be created simultaneously at $t = -12$ ns. As the intensities of the two pulses increase with time, the degree of orientation gradually grows without a significant nonadiabatic transition. From $t = -11$ ns to $t = -8$ ns, 0.78% of the nonadiabatic transition occurs. For the Fig. 4(d) case, by reducing the peak intensity of the ω pulse without controlling the delay between the two pulses, relatively weak alignment with $\langle \cos^2 \theta \rangle \sim 0.5$ is created by the ω pulse at $t = -10$ ns. As the two pulses increase their intensities with time, the molecules start to be oriented. Consequently, even lower 0.33% of the nonadiabatic transition occurs.

In the condition with the higher 2ω laser intensity of 6.0×10^{11} W/cm^2, the physical features investigated for (a), (b), (c), and (d) in Fig. 3(1) are still remaining in (a'), (b'), (c'), and (d') in Fig. 3(2), respectively. However, in the higher 2ω laser pulse intensity, another characteristic condition appears. Being labeled by (e'), the condition provides the almost purely adiabatic molecular orientation. As it is shown in Fig. 6(e'), only 0.26% of nonadiabatic transition has taken place. We call this situation "quasiadiabatic." The condition (e') bears a similarity to (d') in the sense that an adequately weak alignment occurs by only the ω pulse before the orientation is created.

The difference between (d') and (e') in Fig. 3(2) becomes clear by tracing the evolving rotational binding potentials. In Figs. 6(d') and 6(e'), the snapshots of the binding potentials are illustrated. For an easier recognition, the asymmetric term given in Eq. (4) is 100 times exaggerated. In the (d') case,
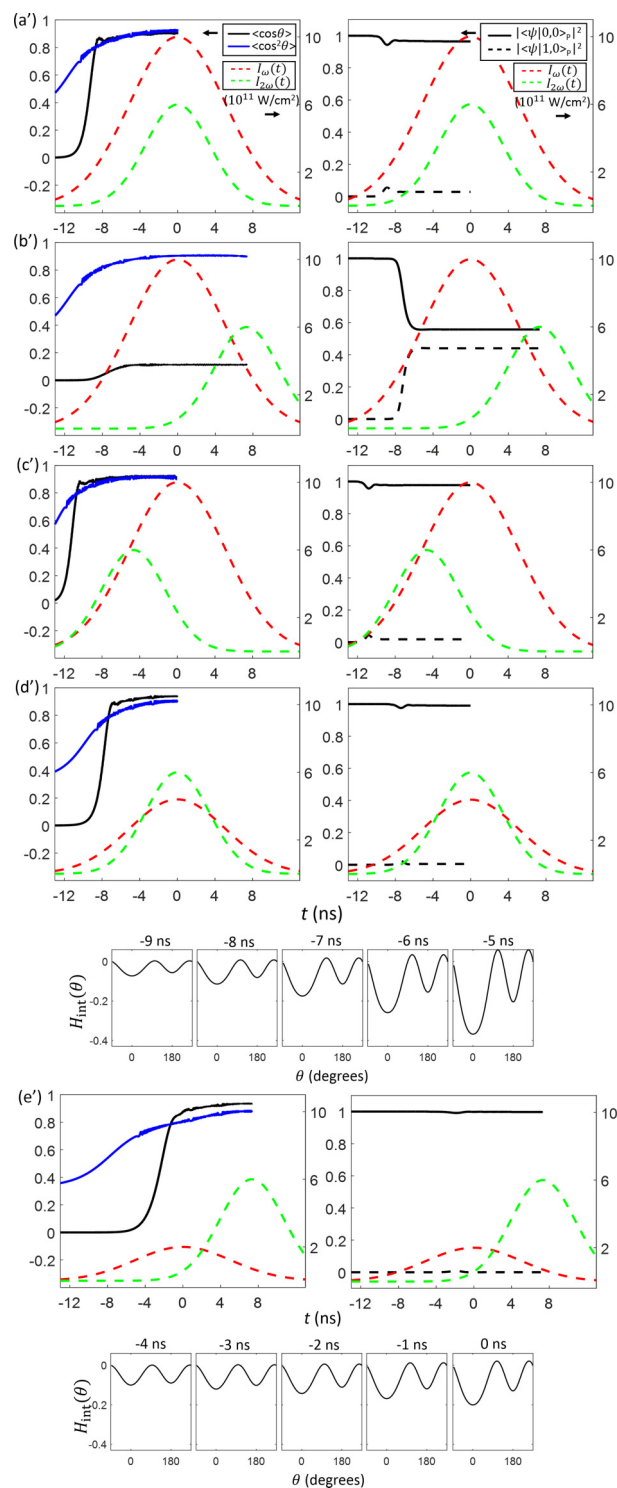
FIG. 6. Temporal evolutions of the degrees of orientation and alignment (left) and populations of two lowest-lying pendular states (right). In the left panels, the left vertical axis of each panel represents $\langle \cos \theta \rangle$ or $\langle \cos^2 \theta \rangle$, while the right vertical axis of each panel represents the intensities of the ω and the 2ω pulses in units of 10^{11} W/cm^2. In the right panels, the left vertical axis represents the populations of the two lowest-lying pendular states, while the right vertical axis of each panel represents the intensities of the ω and the 2ω pulses in units of 10^{11} W/cm^2. The conditions labeled by (a'), (b'), (c'), (d'), and (e') in Fig. 3(2) are employed. For the (d') and (e') cases, the evolving rotational binding potentials are also illustrated.

from $t = -9$ ns to $t = -6$ ns, the depths of the two valleys as well as their depth difference grow while the two intensities of ω and 2ω keep increasing. As a result, 2.68% of the nonadiabatic transition has taken place. In the (e$'$) case, from $t = -4$ ns, the 2ω field starts to interact with the molecules. The laser intensities of the ω and 2ω vary slowly in comparison to the other conditions. Consequently, the rotational binding potential evolves more than two times slower than the (d$'$) case. Under the slowly evolving potential, the wave packet dynamics becomes much closer to the adiabatic process. Within the conditions that we explore, (e$'$) would be the best for achieving higher degrees of orientation

With the rotational ground state of the OCS molecule, we explain that there are several solutions for the quasiadiabatic molecular orientation in the two-color field technique. To generalize the idea, we apply the solutions to the other rotational states. In the tunneling picture of the rotational wave packet, in general, the deeply bound quantum states have smaller probabilities to tunnel through the binding potential than the weakly bound states. Therefore, it is reasonable to expect that the adiabatic orientation of the highly excited rotational states are less demanding. We confirm our recipes toward the adiabatic orientation for the molecules in thermal ensembles.

In Fig. 7, the degrees of orientation (left) and alignment (right) of thermal ensembles are shown. The same conditions labeled by (a$'$)–(e$'$) in Fig. 3(2) are employed. The results from the TDSE and the AA are plotted by solid and dotted lines, respectively. As it is clear, for the alignment, the AA results are in good agreement with the TDSE ones regardless of the laser and molecular conditions. However, for the orientation, the two numerical results show deviation from each other especially for the (a$'$), (b$'$), and (c$'$) cases. The deviation is smaller for higher rotational temperatures because the higher-lying rotational states evolve more adiabatically than the lower-lying states. Based on these results, we conclude that our recipes toward the adiabatic orientation work well for the thermal molecular ensembles.

B. Practical solution toward the adiabatic molecular orientation

In the previous subsection, we explore the conditions toward the adiabatic molecular orientation. However, from the practical point of view, some of those conditions are experimentally demanding because of the long delay between the two laser pulses, for which it is very difficult to stabilize the relative phase between the two wavelengths. Toward the adiabatic orientation without introducing the optical delay, the intensities of the two laser pulses need to be optimized. Figure 8 shows the achieved degrees of orientation and alignment for various laser intensity conditions. These degrees are plotted by contour images as a function of the peak intensities of the ω and 2ω pulses. The alignment results from TDSE and AA are in good agreement with each other. The degree of alignment increases with the total intensity of the two pulses. However, the degree of orientation from the TDSE does not necessarily increase with the total intensity of the two pulses, which is different from the AA results. The contour image from the TDSE indicates that the orientation dynamics approaches the quasiadiabatic situation when the intensity of the 2ω pulse is approximately
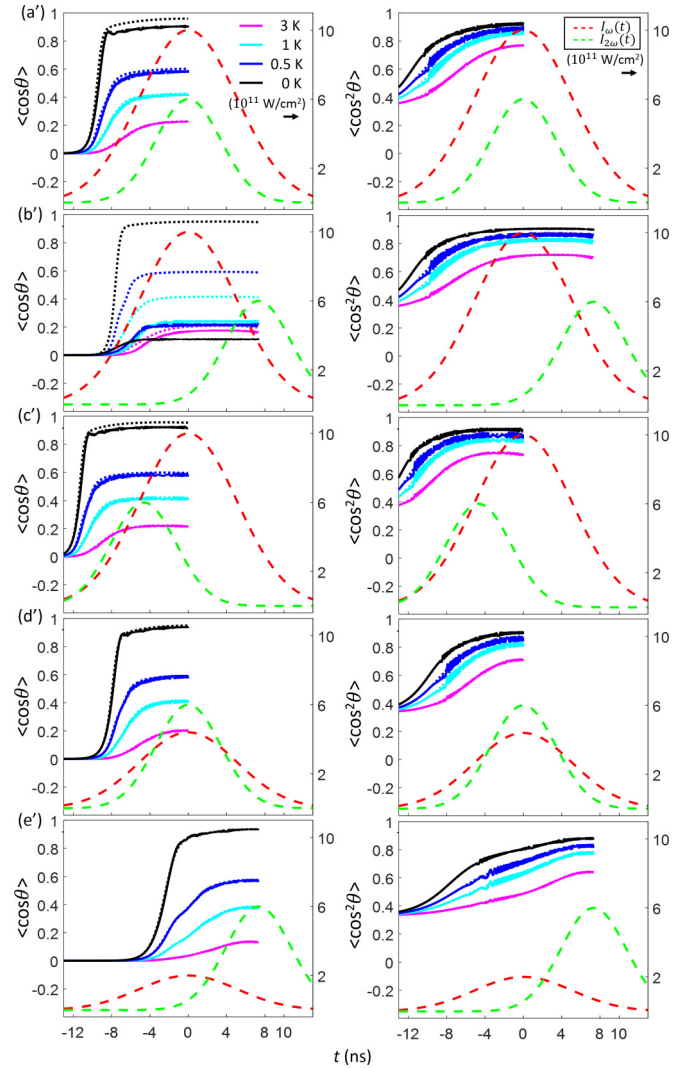
FIG. 7. Time evolutions of the degrees of orientation (left) and alignment (right) of thermal molecular ensembles in the four different rotational temperatures. The solid lines are the results from the TDSE, while the dotted lines are those from the AA. The right vertical axis of each panel represents the intensities of the ω and the 2ω pulses in units of 10^{11} W/cm^2. The conditions labeled by (a$'$), (b$'$), (c$'$), (d$'$), and (e$'$) in Fig. 3(2) are employed.

two times higher than that of the ω pulse as shown by the circle in the upper left panel of Fig. 8.

IV. SUMMARY AND OUTLOOK

In this work, we demonstrate nonadiabatic transitions which decrease the degrees of orientation with the moderately intense nanosecond two-color laser pulse technique. We explain the origin of the nonadiabatic orientation. In the tunneling picture, a rotational wave packet which is confined in a shallower binding potential imperfectly tunnels to the other deeper potential. We show that when the pulse widths of the laser are fixed as constants, by optimizing the intensities and the delay of the two laser pulses, the nonadiabatic transition could be minimized. On the other hand, the condition for the quasiadiabatic molecular orientation requires a delay between
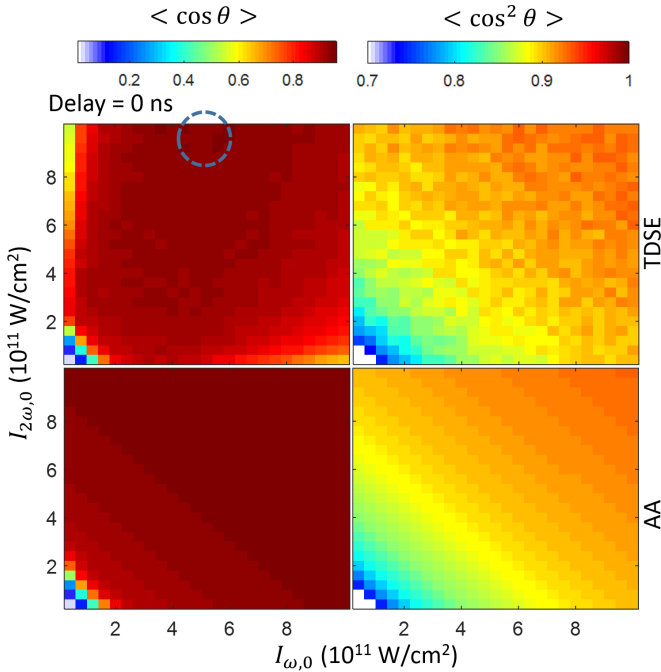
FIG. 8. The degrees of orientation (left) and alignment (right) of the rotational ground state of an OCS molecule. The horizontal and vertical axes are the peak intensities of ω and 2ω pulses, respectively. The delay between the two pulses is set at zero ns. The TDSE and AA results are shown.

the two laser pulses by a several nanoseconds as in the condition (e′) of Fig. 3(2). From a practical (experimental) point of view, without introducing such a long optical delay, the quasiadiabatic molecular orientation can be achieved by optimizing the intensities of the two pulses.

In a recent experiment, a sample of OCS molecules in the rotational ground state was prepared and oriented with the combined-field technique [42]. Theoretically, the quasiadiabatic process can give the maximum degrees of orientation (higher than 0.9) for the ground-state molecules with the two-color laser pulse technique, which has not been achieved experimentally. Once such a high degree of orientation of the ground state is achieved by the two-color field, it is possible to transfer the oriented molecules into the completely field-free condition by applying the plasma shutter technique [33,34,37]. The oriented molecules in the field-free condition would allow us to do various molecular-frame experiments relevant to anisotropic structures of the molecules.

ACKNOWLEDGMENTS

APPENDIX: TIME-DEPENDENT UNITARY TRANSFORMATION METHOD

To compute the rotational dynamics of the molecules, we developed a numerical method. Let us analytically express the time evolution of the rotational wave packet with our method. In a computation, a smooth temporal evolution of the time-dependent Hamiltonian is represented by finite discrete temporal steps. When we look at a single stepwise jump of the laser field due to the finite discrete temporal step, the two frames composed of the eigenstates of the laser-field-dressed Hamiltonians right before and after the stepwise jump can be used for the calculation of time evolution of the wave function. The eigenstates in the two frames are obtained by solving the time-independent Schrödinger equation. The two frames are labeled as (a) and (b), respectively,

$$\hat{H}_a \psi_{a,i} = E_{a,i} \psi_{a,i},$$
$$\hat{H}_b \psi_{b,i} = E_{b,i} \psi_{b,i}, \tag{A1}$$

where $\psi_{a(b),i}$ represents one of the eigenstates of the time-independent Hamiltonian $\hat{H}_{a(b)}$.

We define t_0 to be the moment of the stepwise change of the Hamiltonian from (a) to (b). In general, any wave function can be expressed as a superposition of eigenstates of a time-independent Hamiltonian. It is possible to represent a rotational wave packet at time t_0 by the eigenstates of the Hamiltonian (a)

$$\psi(t_0) = \sum_m c_{a,m}(t_0) \psi_{a,m}, \tag{A2}$$

where $c_{a,m}(t_0)$ are the coefficients of this expansion and $|c_{a,m}(t_0)|^2$ gives the probability of the quantum state $\psi_{a,m}$ at time t_0. For $t > t_0$, until the next stepwise change of the laser intensity, the time evolution of the wave function in the b representation is given by

$$\psi(t) = \sum_{m,n} c_{a,m}(t_0) \langle \psi_{b,n} | \psi_{a,m} \rangle \psi_{b,n} \exp[-i E_{b,n}(t - t_0)]. \tag{A3}$$

In this way, the time evolution of the rotational wave function at $t > t_0$ is obtained by simply adding a phase shift to each eigenstate of $\psi_{b,n}$.

For computing matrix elements of the interaction Hamiltonian and the expectation values of $\cos \theta$ and $\cos^2 \theta$, we use the field-free basis set. In the case of linear molecules, the field-free basis set is spherical harmonics $|J, M\rangle$. The expectation values of $\cos \theta$ and $\cos^2 \theta$ are calculated by using the nonzero matrix elements.

In our numerical method, TDSE is solved exactly without any other approximation except that the laser pulse is given by finite discrete temporal steps. Naturally, by reducing the step size, the calculation becomes more and more reliable. In the present study, the width of the temporal step is set to 20 ps, which has been confirmed to be enough from the convergence of the results. The TDSE calculations were performed with a reasonable numerical cost because of the large temporal step size.

[1] T. Suzuki, S. Minemoto, T. Kanai, and H. Sakai, Phys. Rev. Lett. **92**, 133005 (2004).

[2] J. Itatani, J. Levesque, D. Zeidler, H. Niikura, H. Pépin, J. C. Kieffer, P. B. Corkum, and D. M. Villeneuve, Nature (London) **432**, 867 (2004).

[3] T. Kanai, S. Minemoto, and H. Sakai, Nature (London) **435**, 470 (2005).

[4] T. Kanai, S. Minemoto, and H. Sakai, Phys. Rev. Lett. **98**, 053002 (2007).

[5] C. Vozzi, M. Negro, F. Calegari, G. Sansone, M. Nisoli, S. De Silvestri, and S. Stagira, Nat. Phys. **7**, 822 (2011).

[6] B. Friedrich and D. Herschbach, Phys. Rev. Lett. **74**, 4623 (1995).

[7] B. Friedrich and D. Herschbach, J. Phys. Chem. **99**, 15686 (1995).

[8] T. Seideman, J. Chem. Phys. **103**, 7887 (1995).

[9] H. Sakai, C. P. Safvan, J. J. Larsen, K. M. Hilligsøe, K. Hald, and H. Stapelfeldt, J. Chem. Phys. **110**, 10235 (1999).

[10] J. J. Larsen, H. Sakai, C. P. Safvan, I. Wendt-Larsen, and H. Stapelfeldt, J. Chem. Phys. **111**, 7774 (1999).

[11] T. Seideman, Phys. Rev. Lett. **83**, 4971 (1999).

[12] Z.-C. Yan and T. Seideman, J. Chem. Phys. **111**, 4113 (1999).

[13] C. M. Dion, A. Keller, O. Atabek, and A. D. Bandrauk, Phys. Rev. A **59**, 1382 (1999).

[14] J. Ortigoso, M. Rodríguez, M. Gupta, and B. Friedrich, J. Chem. Phys. **110**, 3870 (1999).

[15] F. Rosca-Pruna and M. J. J. Vrakking, Phys. Rev. Lett. **87**, 153902 (2001).

[16] N. E. Henriksen, Chem. Phys. Lett. **312**, 196 (1999).

[17] B. Friedrich and D. R. Herschbach, Nature (London) **353**, 412 (1991).

[18] H. J. Loesch and A. Remscheid, J. Phys. Chem. **95**, 8194 (1991).

[19] V. A. Cho and R. B. Bernstein, J. Phys. Chem. **95**, 8129 (1991).

[20] B. Friedrich and D. Herschbach, J. Chem. Phys. **111**, 6157 (1999).

[21] B. Friedrich and D. Herschbach, J. Phys. Chem. A **103**, 10280 (1999).

[22] H. Sakai, S. Minemoto, H. Nanjo, H. Tanji, and T. Suzuki, Phys. Rev. Lett. **90**, 083001 (2003).

[23] S. Minemoto, H. Nanjo, H. Tanji, T. Suzuki, and H. Sakai, J. Chem. Phys. **118**, 4052 (2003).

[24] H. Tanji, S. Minemoto, and H. Sakai, Phys. Rev. A **72**, 063401 (2005).

[25] T. Kanai and H. Sakai, J. Chem. Phys. **115**, 5492 (2001).

[26] K. Oda, M. Hita, S. Minemoto, and H. Sakai, Phys. Rev. Lett. **104**, 213901 (2010).

[27] C.-C. Shu, K.-J. Yuan, W.-H. Hu, and S.-L. Cong, J. Chem. Phys. **132**, 244311 (2010).

[28] S. Fleischer, Y. Zhou, R. W. Field, and K. A. Nelson, Phys. Rev. Lett. **107**, 163603 (2011).

[29] K. Kitano, N. Ishii, and J. Itatani, Phys. Rev. A **84**, 053408 (2011).

[30] O. Ghafur, A. Rouzée, A. Gijsbertsen, W. K. Siu, S. Stolte, and M. J. J. Vrakking, Nat. Phys. **5**, 289 (2009).

[31] L. Holmegaard, J. H. Nielsen, I. Nevo, H. Stapelfeldt, F. Filsinger, J. Küpper, and G. Meijer, Phys. Rev. Lett. **102**, 023001 (2009).

[32] F. Filsinger, J. Küpper, G. Meijer, L. Holmegaard, J. H. Nielsen, I. Nevo, J. L. Hansen, and H. Stapelfeldt, J. Chem. Phys. **131**, 064309 (2009).

[33] J. H. Mun, D. Takei, S. Minemoto, and H. Sakai, Phys. Rev. A **89**, 051402(R) (2014).

[34] D. Takei, J. H. Mun, S. Minemoto, and H. Sakai, Phys. Rev. A **94**, 013401 (2016).

[35] M. Muramatsu, M. Hita, S. Minemoto, and H. Sakai, Phys. Rev. A **79**, 011403(R) (2009).

[36] Y. Sugawara, A. Goban, S. Minemoto, and H. Sakai, Phys. Rev. A **77**, 031403(R) (2008).

[37] A. Goban, S. Minemoto, and H. Sakai, Phys. Rev. Lett. **101**, 013001 (2008).

[38] J. J. Omiste and R. González-Férez, Phys. Rev. A **88**, 033416 (2013).

[39] J. J. Omiste, R. González-Férez, and P. Schmelcher, J. Chem. Phys. **135**, 064310 (2011).

[40] J. L. Hansen, J. J. Omiste, J. H. Nielsen, D. Pentlehner, J. Küpper, R. González-Férez, and H. Stapelfeldt, J. Chem. Phys. **139**, 234313 (2013).

[41] J. H. Nielsen, P. Simesen, C. Z. Bisgaard, H. Stapelfeldt, F. Filsinger, B. Friedrich, G. Meijer, and J. Küpper, Phys. Chem. Chem. Phys. **13**, 18971 (2011).

[42] J. H. Nielsen, H. Stapelfeldt, J. Küpper, B. Friedrich, J. J. Omiste, and R. González-Férez, Phys. Rev. Lett. **108**, 193001 (2012).

[43] G. Maroulis and M. Menadakis, Chem. Phys. Lett. **494**, 144 (2010).